Thermostimulated crystal structure transformation of the polymineral clay submicron particles

A. G. Chetverikova[1], O. N. Kanygina[1], V. N. Makarov[1], V. L. Berdinskiy[1], M. M. Seregin[2]*
[1]Orenburg State University, Orenburg, Russian Federation
[2]LLC "Lumex-Centrum", Moscow, Russian Federation

Abstract

Changes in the structure of phyllosilicate microparticles of submicron fractions of polymineral clay with an average size of 290 nm, as well as changes in the positions of impurity ions of transition metals in the crystal lattice, were studied by X-ray diffraction analysis, Fourier transform infrared spectroscopy, and high-resolution electron paramagnetic resonance spectroscopy. The main composition of microparticles included clinochlore, montmorillonite, calcite, and quartz. Structural transformations were stimulated by heating the samples to 1200 K at a rate of 10 K/min. A decrease in the number of crystal structures of microparticles was recorded due to the amorphization of montmorillonite, the decomposition of calcite, and the formation of sillimanite. Structural rearrangements of crystal cells containing impurity paramagnetic ions Fe^{3+} and Mn^{2+} in submicron particles of clinochlore and montmorillonite, accompanied by displacements and changes in the chemical bonds of these ions, were recorded by the ion-electron paramagnetic resonance method. It is shown that when microparticles were heated to 1200 K, the impurity paramagnetic ions of transition metals did not go beyond their crystal cells.
Keywords: phyllosilicate particles, structure, paramagnetic ions, spin labels.

INTRODUCTION

Finely dispersed oxide powders with microparticle sizes of less than 1 μm are used to obtain special ceramics (for example, corundum and quartz ceramics). The preparation of raw materials in this case is a complex economically and energy-consuming problem. The problem of obtaining special ceramics from ultrafine powders of natural clays is becoming more and more urgent. Polymineral clay powders can serve as the main raw materials for new ceramics, and high-temperature firing, which leads to sintering and significant structural rearrangements of phyllosilicate microparticles, changing their physical and chemical properties and operational characteristics, can be a common technological method. Polymineral (PM) clays are the most common in the world. Their main minerals are phyllosilicates: disordered kaolinite or montmorillonite, chlorite, and illite. Impurities are traditionally represented by quartz and organic matter. Phyllosilicates (in particular, illite) are very susceptible to transformations when ground to submicrometric sizes. The description of natural minerals with great variations of dispersion, compositions, isomorphism, and polymorphism requires a special approach each time. An important preliminary stage in the production of various ceramic materials is the grinding and fractionation of natural polymineral clays; small fractions significantly improve the quality of products. Phyllosilicates (in particular, illite) are very susceptible to transformations during grinding: for example, with an increase in their dispersion, Fourier transform infrared (FTIR) spectroscopy shows a change in absorption bands [1].

Polymineral clays often contain ions of various metals, including rare and scattered chemical elements. The entry of such ions into the crystal lattices of phyllosilicates as impurities of introduction or substitution makes their extraction a difficult, energy-consuming, and expensive procedure. Knowledge of the state of impurity ions of transition metals in the crystal cells of microparticles of silicate materials is a necessary element for the development of techniques for their extraction. On the one hand, the complex composition of natural polymetallic clays increases the number of their useful qualities and properties in comparison with 'pure' synthesized materials. On the other hand, it aggravates studying them by various physico-chemical methods and requires research and knowledge of the properties of their microparticles containing a minimum amount of constituent minerals and substances. It is possible to reach a fundamentally new level of determining the structure of complex natural ultrafine systems, including polymineral clays, only with the use of a complex of precision research methods [2].

The purpose of this study was to establish structural transformations occurring in ultrafine particles of clay minerals at different hierarchical levels. In this study, from a variety of polymineral clays, one consisting mainly of chlorides with a low content of montmorillonite (without kaolinite) was selected. The chemical composition of such clays is variable; the most characteristic is the presence of iron, calcium, and magnesium oxides in them [3]. The mineral varieties in the chlorite group are explained by a wide isomorphism, i.e. the ability to replace both individual atoms and extended lattice fragments, which causes

**KR-727@mail.ru*
https://orcid.org/0000-0002-7045-3588

significant variations in its chemical composition [4]: $(Mg,Fe)_{6-x-y}(Al,Fe)_{x+2y/3}(Si_{4-x}Al_xO_{10})(OH)_8$, where the value of x for ferruginous chlorites varies from 1.6 to 2. If the divalent Mg^{2+} cations are replaced by divalent Fe^{2+} cations according to the atom-by-atom scheme, then the structure of the so-called clinochlore is formed. Its octahedral (O) layers, unlike tetrahedral (T), can be populated with small amounts of divalent Mn^{2+} and Zn^{2+} cations. Such structural transformations distort the lattice, reducing the size of octahedra [4]. The ideal structure of montmorillonite is similar to the layered (T-O-T) structure of chlorite and is described by the formula $Al_4Si_8O_{20}(OH)_4.nH_2O$. The average structural formula of real minerals of this type is as follows [5]: $K_{0.33}[Al_{1.67}(Fe^{2+},Mg)_{0.33}][Si_{3.95}(Al,Ti)_{0.05}]O_{10}(OH)_2.nH_2O$. In both natural minerals, the octahedral layer usually contains spin tags - paramagnetic ions of iron and manganese.

EXPERIMENTAL

It is logical to interpret the results of any analysis of natural raw materials only after the extraction of clay minerals [3]. The most common method is deposition. It is known that the proper sizes of clay particles lie in the nanometer range. Therefore, if one sets the upper limit of the fine fraction equal to 0.25 μm, it is almost completely represented by clay minerals. Coarse-grained minerals, such as quartz, calcite, magnetite, corundum, and others go into a large fraction in this case. The dried natural clay was ground using a planetary ball mill (PM400, Retsch). 10 g of clay were ground in a 200 mL ceramic beaker containing corundum grinding balls. Clay samples were ground for 1 h at a frequency of 300 rpm. After sieve screening of the washed polymineral clay, a fraction with particle sizes less than 4 μm was selected for research.

Granulometric composition of polymineral clay was determined by the laser diffraction method (photon correlation spectroscopy) on a particle size analyzer (Compact-Z, Photocor, Russia). Powders after ball milling with a d≤4 μm in size were suspended in a dispersion medium (deionized water). Ultrasonic dispersion of the suspension was carried out for 5 min using an ultrasonic homogenizer. To achieve stability, the suspension was settled for 300 min under free sedimentation conditions. Immediately before the analysis, the suspension was diluted using a similar dispersion medium until the required concentration of 1 wt% was reached. The hydrodynamic diameter of nanoparticles in each sample was measured twice under thermostatically controlled conditions at 21.0±0.5 °C by photon correlation spectroscopy in accordance with a certified measurement technique [6]. Next, the electrokinetic potential was measured by their electrophoretic mobility on an analyzer (Compact-Z, Photocor). Considering the type of sample, a cell with immersed electrodes was used; the applied voltage was 5 mV and the interelectrode space was 4 mm [7, 8]. The specifics of the experiment are described in detail elsewhere [9]. For statistical analysis of a group of particles, the samples were scanned using an atomic force microscope (SMM-2000, Proton-MIET, Russia) in contact mode using general-purpose cantilevers (MSCT, Bruker, USA) with a rigidity of 0.01 N/m and a nominal radius of curvature of the probe of 15 nm. The microscope software was used for morphometric analysis of the obtained images. An insignificant amount of clay suspensions was applied on a fresh cleavage of mica as the substrate. After complete drying, the samples were scanned at a speed of 1 line/s.

Chemical composition of the ultrafine (less than 1 μm) clay fraction was determined using silicate and X-ray fluorescence analyses. The following metrics were determined in a standard pre-weighed sample according to an interstate standard [10]: moisture content, mass loss on ignition (LOI), silicic acid content, the sum of 'sesquioxides' (Al_2O_3+Fe_2O_3+MnO+TiO_2), and separately the mass fractions of iron, aluminum, calcium, and magnesium oxides. The mass loss was determined by an indirect method after calcination of a preweighed amount, 100 g (±0.0001 g) dried at 110 °C, in 3 h at 1000 °C. Free silica was determined by isolating insoluble SiO_2 using hot phosphoric acid and then calcining it to constant weight. Iron oxide (III) was determined by photometric method with sulfosalicylic acid and titanium oxide (IV) with hydrogen peroxide. The complexometric method gave the value of alumina without the separation of silicon oxide (IV). The flame spectrometric method determined the oxides of potassium and sodium. All determinations were made in parallel specimens, and the error of analysis (±0.0002 g) was taken into account in the conversion. Besides, the elemental composition of the metals in clay was determined using an X-ray fluorescence crystal-diffraction scanning spectrometer (Spektroskan LF, Spektr, Russia). LiF was the analyzer crystal. The anode material of the X-ray tube was Ag. The standby voltage and current were 40 kV and 100 μA, respectively. The range of motion of a crystal did not exceed 3190 mÅ. The content of Cu, Zn, and Mn was determined by means of atomic absorption spectroscopy (Spektr 5, Zelaz, Russia), in accordance with the M-MVI-80-2008 standard. The obtained values were converted to the oxides of the corresponding metals and corresponded to previous results.

Phase composition of the powders was studied by X-ray phase analysis using a diffractometer (Diffray-401) in monochromatized cobalt radiation at a rate of 2.5 deg/min. The reflexes were indicated on the diffractogram using LookPDF software, which allowed us to index X-ray diffraction (XRD) patterns using ICDD Powder Diffraction File data. *FTIR spectra* were recorded on a spectrometer (InfraLUM Ft-08, Lumex) with an optical system made of potassium bromate. The spectrometer was equipped with an add-on of disturbed total internal reflection (DTIR) with a zinc selenide crystal, which allows for analyzing samples in liquid and solid aggregate states. The measurements were carried out in accumulation mode for 120 s. The spectral range was from 525 to 4000 cm^{-1} in increments of 4 cm^{-1}. Before each measurement of the samples, the background spectrum of the add-on was evaluated. Then a powder sample was placed on the crystal

surface under high pressure. After removing the spectrum of the sample, the crystal was cleaned with cotton wool soaked in acetone.

Electron paramagnetic resonance (EPR) spectra of clay samples were recorded on a small-sized automated spectrometer (CMS8400 EPR) at room temperature. The conditions for recording EPR spectra were similar to those given in the study of Kanygina et al. [11]: frequency of 9.86 GHz, magnetic field of 1-7 kOe, modulation of the magnetic field with a frequency of 100 kHz, and amplitude of 6 G. Structural transformations in clay minerals were initiated by resistive heating. *Differential thermal analysis* (DTA) was performed to study the processes of restructuring and amorphization of the crystal lattice of polymineral clay. The derivatograms were taken on an apparatus (Thermoscan-2) with a heating rate of 10 K/min. The heating conditions were selected so that there was no sintering or agglomeration of particles. The error in determining the temperature was ±1 K. Aluminum oxide powder (Al_2O_3) weighing 0.5 g, sealed in a quartz vessel, was used as a reference. The weight of the polymineral clay sample before the experiment was 0.5 g.

RESULTS AND DISCUSSION

Granulometric composition of the dispersed system (meso-level): the main condition for obtaining reliable particle size distributions was the preparation of a colloidal clay suspension that prevented active flocculation of particles. First, the dependence of the electrokinetic (ζ) potential on the pH of the suspension was established. The isoelectric point of the colloidal suspension of polymineral clay (-0.3 mV<ζ-potential<0.2 mV) corresponded to pH 1.5. This acidity was supposed to balance the processes of dispersion and aggregation of particles. The distribution of particles in 4 fractions is shown in Fig. 1. The first group of particles (1.4%) with a size of 0.7±0.2 nm was probably represented by montmorillonite. The true sizes of its native particles were about 1 nm [12]. The second group (24.7%) with dimensions of 300±50 nm corresponded to smectite particles. The third group (38%) of the micrometric range (d=4.8±1.4 μm) was formed by microaggregates of phyllosilicates or quartz particles. Finally, the last group (36%) was the most unstable, consisting of periodically formed flakes.

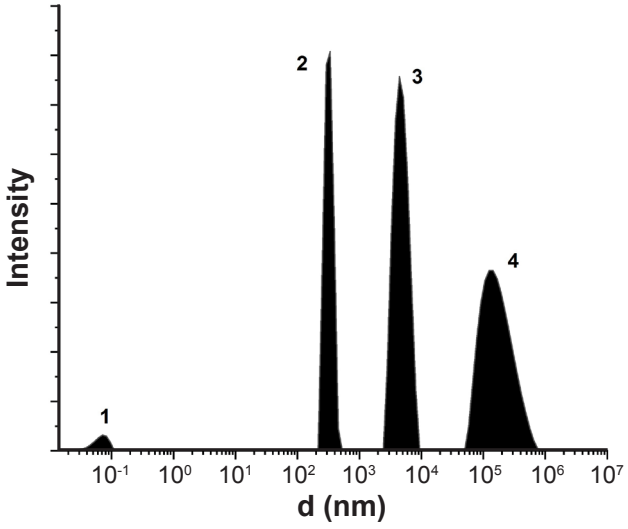

Figure 1: Particle size distribution curve of clay powders by laser diffraction method (pH=1.5).

Fig. 2b, an overview scan of the sample, shows two fractions of particles: a scattering of submicrometric objects 120-520 nm in size is visible; in the lower part of the image there is an object with a height of more than 3 μm. Fig. 2c shows a frame with an isometric microparticle typical of quartz. On the left (Fig. 2a) is an optical image of polymineral particles after grinding in a ball mill. The results of the statistical AFM analysis on a section with a length of 10 μm are shown in Fig. 3. The red line corresponds to the average probable value of particle size of 290 nm. In the right part of the figure, there is a histogram of the particle size distribution along the secant. It can be seen that the size of the particle clusters varied from units to 700 nm, half of them had medium-probability sizes, correlating with the results of photon correlation spectroscopy (the first two groups).

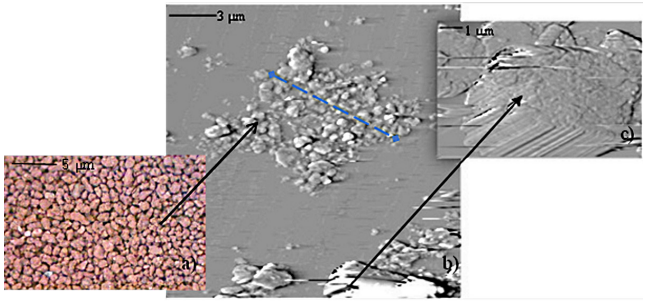

Figure 2: Images showing particle scattering: a) optical image of the dried powder after grinding in a ball mill; and b,c) AFM images of particles deposited on a mica substrate. Frame b shows one of the secants along which the morphometric analysis of particles was performed.

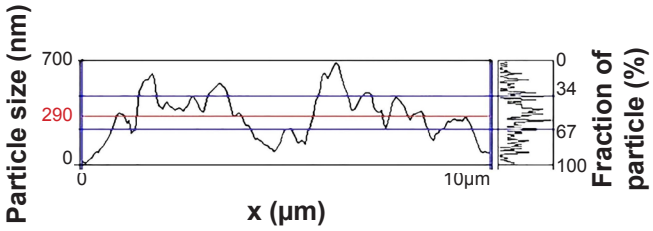

Figure 3: Morphometric statistics of particles along a 10 μm secant.

Chemical composition of native particles: the chemical composition of the ultrafine fraction less than 4 μm (the first two groups) is shown in Fig. 4. According to the classification given by Chen et al. [13], polymineral clay refers to acidic clays with a high content of coloring oxides, free silica, and water-soluble salts of Na and K. Such compositions are characteristic of polymineral clays of the Orenburg Region (Russia) [14].

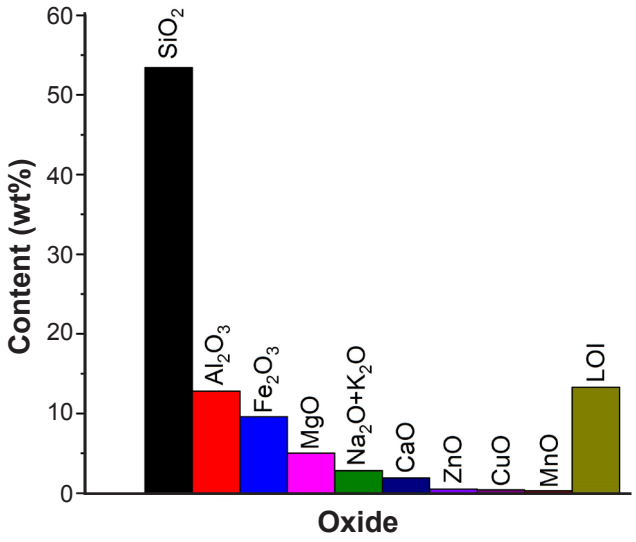

Figure 4: Chemical composition of polymineral clay as determined by X-ray fluorescence spectroscopy and chemical (silicate) analysis.

Results of differential thermal analysis: derivatography of clays of the Orenburg Region was carried out earlier elsewhere [15, 16]; however, the clays of the Novoorskoye deposit were described in these studies. The results of the thermal analysis of this polymineral clay have not been published before. The derivatogram describing thermal effects in polymineral clay is shown in Fig. 5. During heating, the sample lost about 11% of its mass, which indicated significant structural transformations, primarily due to the decomposition of components. The first endothermic effect (label a) in the temperature range from 320 to 570 K (with a maximum at 420 K) was interpreted as the decomposition of organic substances and removal of absorption-bound (hydrate) and interlayer molecular water of phyllosilicates [17]. The second endothermic effect (label b) in the temperature range of the sample from 570 to 870 K was due to the removal of crystallization water from montmorillonite and chlorite with partial amorphization of the ceramic mass [3, 17]. A similar effect at lower temperatures was observed when the microwave field irradiated montmorillonite samples in a humid environment [18]. Heating from 870 to 1120 K did not cause visible changes in this range. In the range from 1120 to 1170 K, an intense third endothermic effect (label c) was observed with a maximum at 1160 K.

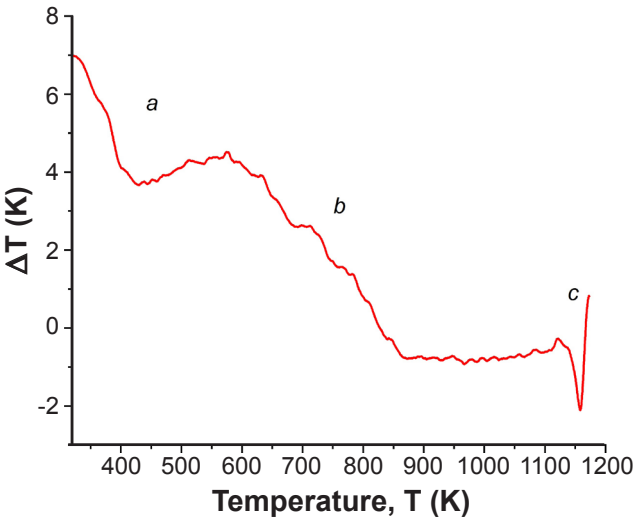

Figure 5: Derivatogram of polymineral clay.

Transformation of the crystal structure (microlevel): according to the results of X-ray phase analysis, the polymineral clay included 7 crystalline phases, the main share of which fell on ferruginous chlorite (46%), montmorillonite (15%), and β-quartz (15%). The content of the remaining phases (MgO, Al_2O_3, $CaCO_3$, and Fe_3O_4) did not exceed 10%. The qualitative phase composition of natural particles is shown in Fig. 6. The interplanar distances of the main reference lines of quartz reported by Kukartsev et al. [19] coincided with our data. The quantitative phase compositions of polymineral clay before and after DTA are shown in Table I. As in the study of Baratian et al. [20], based on the Fenner diagram with respect to MgO, the amount of magnesium oxide in polymineral clay correlated with the content of free quartz, alumina, and iron oxide. In contrast to the representative soils of Brazil with low, high, and medium concentrations of iron oxides (including oxides and oxyhydroxides - goethite α-FeOOH, hematite α-Fe_2O_3, maghemite γ-Fe_2O_3, and magnetite Fe_3O_4, which was the main clay mineral) considered by Barbosa et al. [21], only magnetite was present in our clay in a small amount. According to the results of X-ray phase analysis, the number of crystal structures after DTA decreased by 35% due to the complete amorphization of montmorillonite and calcite decomposition [22]. Probably, at this stage, isomorphic substitutions in clinochlore with the activation of ions of the hydroxyl group bound to magnesium took place [23]. Energy consumption was also required by the formation of a new aluminosilicate - sillimanite. The contents of other oxides did not change (Table I).

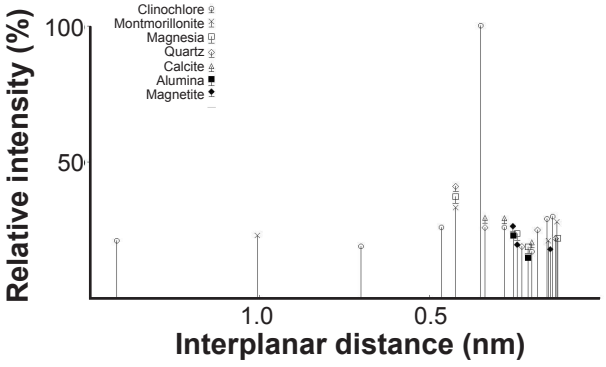

Figure 6: XRD results of natural polymineral clay.

Bands corresponding to minerals such as hematite, quartz, calcite, clinochlore, and montmorillonite were seen in the FTIR absorption spectrogram (Fig. 7) of the initial sample (Table II). The main contribution to the absorption

Table I - Quantitative phase composition of clay.

Phase	Fraction at initial state (vol%)	Fraction after DTA (vol%)
Clinochlore [ferruginous chlorite, $(Mg_{4.8}Fe_{0.92})Al_{0.25}(Si_{2.83}Al_{1.17})O_{10}(OH)_8$]	46	17
Montmorillonite [$Al_2(OH)_2Si_4O_{10}.mH_2O$]	15	-
Silica (SiO_2)	15	15
Magnesia (MgO)	7	7
Alumina ($Al_2O_{3)}$	5	5
Magnetite ($Fe_3O_{4)}$	6	5
Calcite ($CaCO_3$)	6	-
Sillimanite ($Al_2O_3.SiO_2$)	-	16
Integral intensity, I	100	65

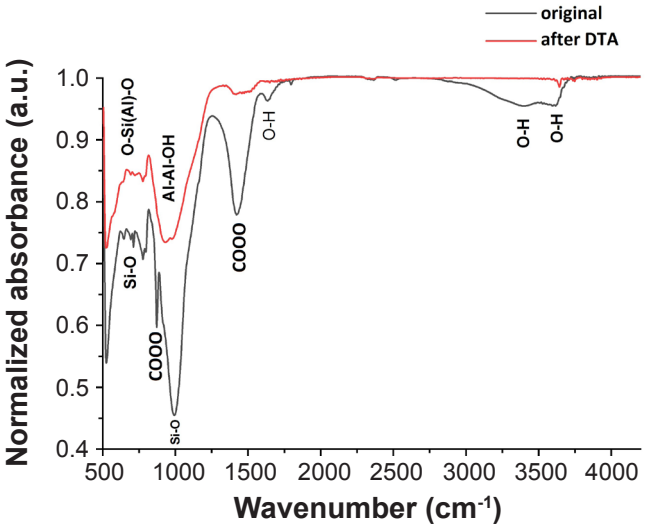

Figure 7: FTIR spectra of clay in the initial state and after DTA.

of infrared radiation was made by montmorillonite and clinochlore, whose bands mostly overlap, which created the problem of their simultaneous determination. Hydrated water deserves special attention; its wide lines of valence and deformation vibrations appeared at 1635 and 3386 cm^{-1}. The 3621 cm^{-1} band can be attributed to the valence symmetric bonds of internal OH groups located in a plane common to octahedral and tetrahedral layers. With the partial substitution of silicon in the lattice, most of the valence bands of layered minerals in the range from 1000 to 900 cm^{-1} moved towards low frequencies [24]. The appearance of absorption bands in this region may be associated with valence vibrations of non-bridge Si-O bonds in various silicate and aluminosilicate groupings, as well as in simple ortho- and diorthosilicate anions in the amorphous phase. The main Si-O vibrational bonds of montmorillonite at 992 cm^{-1} corresponded to the bonds at 833 and 915 cm^{-1}, which correspond to the substitution of aluminum and magnesium in the octahedral silicon layer. In such phyllosilicates, the presence of a very weak 912 cm^{-1} band was explained by the manifestation of deformation vibrations of the non-bridge Al-O-H bond, which is much longer and weaker than the Si-O bond. As a rule, another bond corresponding to iron substitution is present in the spectrum of montmorillonite [25]; however, in this case, it overlapped with the absorption band of calcite at 872 cm^{-1}.

Very weak bands at 797 and 694 cm^{-1} in the samples can be explained by Si-O-Si (Al) bonds in distorted tetrahedral and octahedral layers. In particular, the band of 694 cm^{-1} referred to the deformation vibrations of Si-O-Si, including bridged oxygen, and the band of 797 cm^{-1} referred to the valence symmetric vibrations of Si-O-Si, specific to silicon in the SiO_4 tetrahedron. The mode of 530 cm^{-1} was identified as the oscillation of FeO groups of magnetite. The modes of interlayer water in montmorillonite and clinochlore disappeared in the FTIR spectrogram after DTA (Fig. 7). The remaining O-H groups were represented by a narrow band at 3640 cm^{-1} remaining after the ordering of hydroxyl groups in the crystal lattice of clinochlore. The modes of COOO oscillations disappeared after DTA, which indicated a partial decomposition of calcite. A decrease in the intensity of Si-O bond oscillation in montmorillonite was noted in comparison with Al-Al-OH oscillations, as well as the appearance of Al-Fe-OH modes. The absorption bands of aluminosilicates were shifted by wavenumbers; therefore, the structures of montmorillonite and/or clinochlore transformed. Using the 530 cm^{-1} band, it was difficult to assess the changes that occurred in the magnetite, since its main absorption lines were outside the range of measurement capabilities of the DTIR add-on.

Structural transformations of crystal cells with substitution ions (nanoscale): the presence of paramagnetic metal ions Fe^{3+} and Mn^{2+} in the form of substitution impurities in the crystal lattice of the finely dispersed montmorillonite fraction opens up great opportunities for their use as natural spin probes and the EPR method. It is known that Fe^{3+} ions, as well as ions of other transition metals, are capable of replacing Al^{3+} ions in the octahedral system of phyllosilicates and are not embedded in the tetrahedral system with the substitution of Si atoms [31]. The overview EPR spectra

Table II - Characteristic modes of interatomic bonds in PM samples in the initial stage and after DTA exposure.

Mode of the initial substance (cm^{-1})	Mode after DTA (cm^{-1})	Type of oscillation	Mineral	Ref.
530	530	Fe-O	Magnetite	[26]
645	645	O-Si(Al)-O	Montmorillonite, clinochlore	[27]
694	694	Si-O	Quartz	[28, 29]
712	-	COOO	Calcite	[30]
777	777	Si-O	Quartz	[28]
796	798	Si-O	Quartz	
833	846	Al-Mg-OH	-	[30]
872	-	COOO	Calcite	
-	877	Al-Fe-OH	Montmorillonite	[25]
915	931	Al-Al-OH	Montmorillonite, sillimanite	
992	982	Si-O	Montmorillonite, clinochlore, sillimanite	[24, 25, 27]
1421	1421	COOO	Calcite	[26, 30]
1635	-	O-H (water)	Montmorillonite, clinochlore	[25, 27]
3386	-	O-H (water)	Montmorillonite, clinochlore	[25, 27]
3620	3640	O-H	Montmorillonite, clinochlore	[25, 27, 29]

of the fine fraction of the nanometer range before and after DTA are shown in Fig. 8. A set of narrow lines in the region in the magnetic field B≈345 mT and with the g-factor g≈2.0 belongs to Mn^{2+} ions. A wide line in the same spectral region with g=2.0018 belongs to iron ions in the composition of the ferrimagnet Fe_3O_4, whose fine particles exhibit the properties of a superparamagnet. Therefore, the line with g=2.0018 was identified as the magnetic resonance line of superparamagnetic Fe_3O_4 particles. In the literature, such spectra are sometimes called superparamagnetic resonance spectra [32]. Strong exchange interactions within the particles build the electron spins of Fe^{2+} and Fe^{3+} ions, which behave like unusual paramagnets in a magnetic field. EPR spectra of Fe^{2+} ions are not observed under normal conditions, as a rule. Fe^{3+} ions containing 5d-electrons can be in the high-spin state (S=5/2) and in the low-spin state (S=1/2) depending on the symmetry of the crystal environment. In the initial state (Fig. 8a), a wide (21.6 mT) asymmetric line with an isotropic g-factor of 4.0889 was observed in a weak magnetic field (B≈160 mT), which indicated a strong trigonal distortion of the crystallographic environment of the Fe^{3+} ion. Roasting at a high temperature of 1200 K changed the width and shape of this magnetic resonance line. After DTA (Fig. 8b), the line width decreased approximately 2.5 times (8.4 mT), and the value of the g-factor reached 4.2008. The amplitude of this line decreased compared to the amplitude of the wide (second) line with a g-factor of ~2.00. The change in the amplitude indicated that during the roasting process, Fe^{3+} ions moved to a low-spin state with S=1/2, specific for a symmetrical crystallographic environment.

The resonant signal at sextet lines was observed above the wide superparamagnetic resonance line in the region of g≈2.0, specific for the EPR spectrum of Mn^{2+} ions. For reliable separation of wide and narrow lines, the recording mode of the second derivative $\partial^2\chi''(H)/\partial H^2$ of the EPR spectrum $\chi''(H)$ was used [33]. In this recording mode, the wide lines of the 'first derivative' $\partial\chi''(H)/\partial H$ in the constant slope region gave a small addition, and the narrow lines of the first derivative provided narrower lines in the spectrum of the 'second derivative'. Such EPR spectrum of polymineral clay microparticles in the initial state in a narrow region with a g-factor of ~2.00 is shown in Fig. 8d. It is represented by characteristic six lines of Mn^{2+} ions and a set of doublets of different intensities, as well as two single lines. The intensity of the sextet lines in the original clay monotonously decreased toward strong magnetic fields. This was due to the partial coincidence of the spectra of two types of Mn^{2+} ions located in crystallographically unequal positions. The locations of the extreme left lines of the manganese sextets in these positions coincided. Small discrepancies between the g-factors and the hyperfine coupling constants led to a shift in the positions of the remaining sextet lines and a

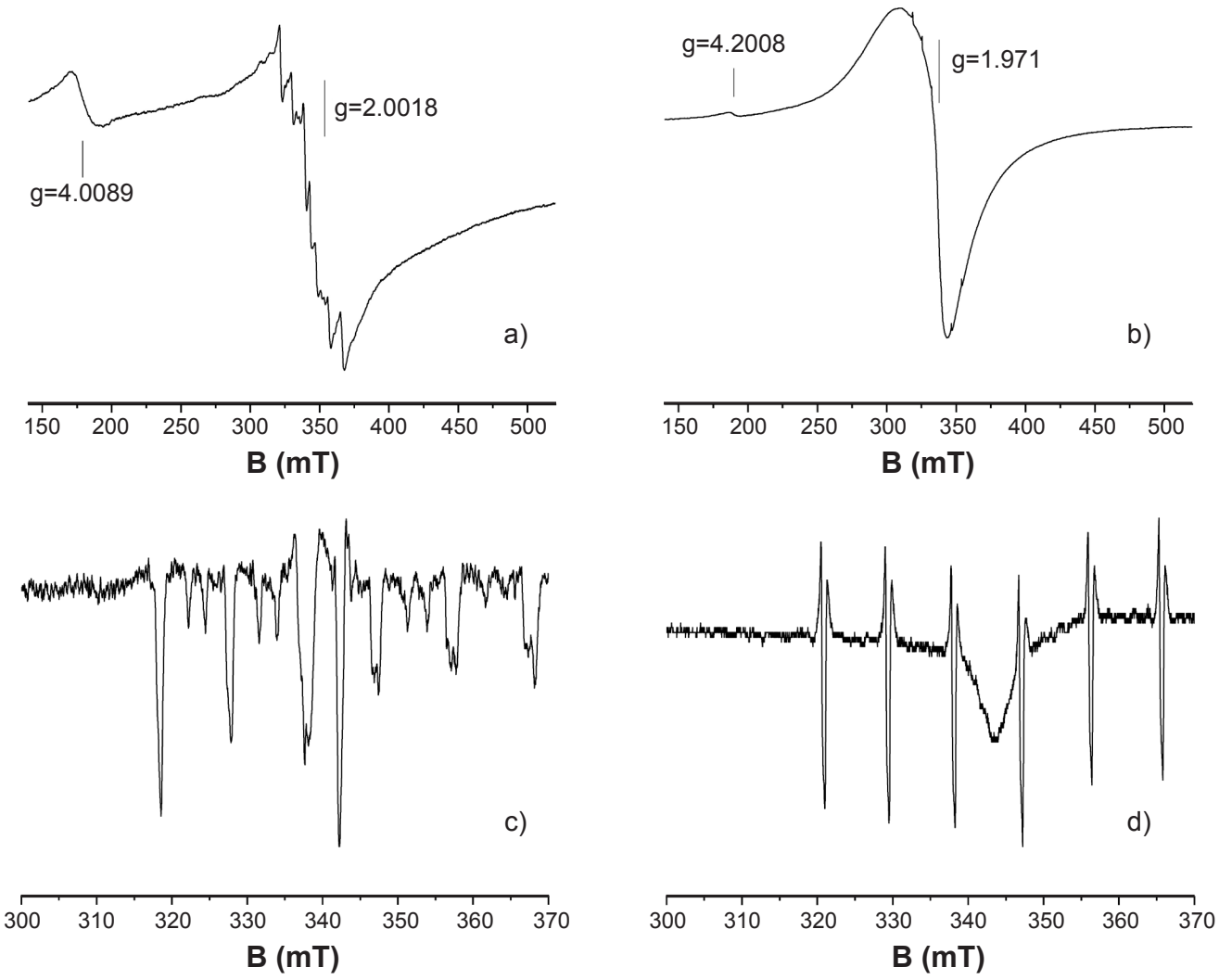

Figure 8: Overview EPR spectra of clay in the initial state (a) and after DTA (b), and the second derivative of the EPR signal of the manganese ion in the initial state (c) and after DTA (d).

sequential decrease in their total amplitudes so that the right line of the spectrum (in a 'strong' magnetic field) split into two. Comparing the amplitudes of these components with the amplitude of the non-split line, it can be concluded that Mn^{2+} ions were in two equally probable positions in the octahedral lattice, interacting with oxygen ions (Figs. 9a and 9b). The amplitudes and positions of the sets of doublet lines in the intervals between the components of Mn^{2+} ion sextets indicated that these lines also belonged to Mn^{2+} ions, whose unpaired electrons additionally interacted with the nuclei of hydrogen atoms (nuclear spin I=1/2) of hydroxyl groups (Fig. 9c). The totality of the results obtained made it possible to imagine the possible arrangement of nonequivalent Mn^{2+} ions inside a chlorite crystal cell along three types of octahedron vertices formed by oxygen atoms. The first two types corresponded to a pair of oxygen atoms equidistant from OH groups, and the third type corresponded to the hydroxyl group O-H. After DTA (Fig. 8b), there were narrow, well-resolved lines of Mn^{2+} ions identical in amplitude to the second derivative in the EPR signal. Consequently, in the dispersed system, all manganese ions occupied an equilibrium position relative to oxygen atoms inside the crystal cell, forming strong chemical bonds. The doublet splitting disappeared simultaneously with OH groups that gave rise to it. Unfortunately, the accuracy of modern quantum chemical calculation methods did not allow unambiguously to identify the listed types of nonequivalent Mn^{2+} ions according to EPR spectra.

Signals associated with local defects are usually observed in EPR spectra of phyllosilicates: narrow lines in the region g≈2.0 (Figs. 8c and 8d) [34, 35] caused by electron-hole centers that arose during isomorphic substitutions of cations in the O-layer. The position of the first of them coincided with one of the components of the sextet. The second signal from defects was characterized by a g-factor of 1.9775, i.e. from O^- centers that were stabilizers of $Mg^{2+} \rightarrow Al^{3+}$ substitution [36]. They are weakly related to the structure of the mineral and served as indicators of the influence of temperature on the structural ordering of the mineral. After roasting, the signal from the defects disappeared as

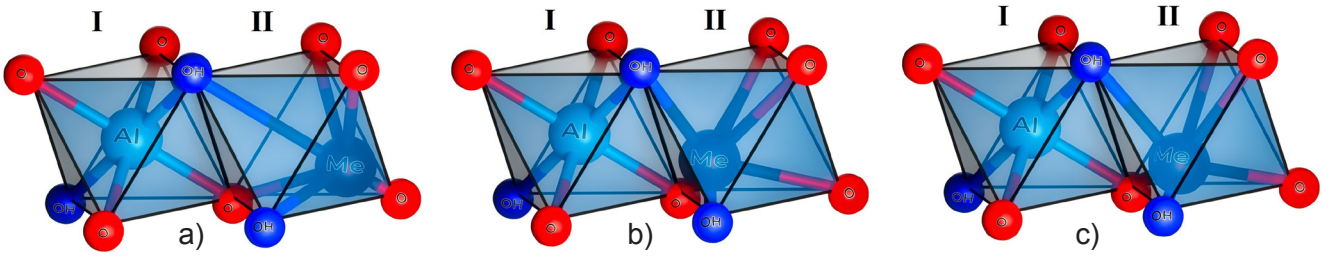

Figure 9: Oxygen octahedra of phyllosilicates, where I is an ideal octahedron and II is an octahedron in which Al^{3+} is replaced by Fe^{3+} or Mn^{2+} with different arrangements of impurity ions.

expected. Parallel registration of changes in EPR spectra of two spin probes (Fe^{3+} and Mn^{2+} ions) after heating to 1120 K indicated significant changes in the structure of crystal cells containing impurity ions.

CONCLUSIONS

Structural transformations in polymineral clay particles with an average probable value of 290 nm, occurring during heating to 1200 K at a rate of 10 K/min, were experimentally studied. Thermal stimulation led to structural transformations at the microscopic and submicroscopic (nanometric) levels. At the microscopic level, phase transformations occurred, which included the decomposition of montmorillonite and calcite, partial amorphization of clinochlore, and the formation of sillimanite. The presence of paramagnetic ions Fe^{2+}, Fe^{3+}, and Mn^{2+} in natural polymineral clay gave a unique opportunity to register their environment in native clay and after differential thermal analysis (DTA). Electron paramagnetic resonance (EPR) spectroscopy made it possible to see the structural changes of the nano level that were not registered by other methods. Using the second derivative of the signal, the presence of various Mn^{2+} crystal chemical positions in the octahedron of phyllosilicates was established. After the DTA, the signal intensity of the Mn^{2+} sextet lines leveled off, i.e. manganese ions occupied a more equilibrium position in the crystal lattices. The content of Fe^{3+} ions inside the distorted crystallographic cells changed during the roasting process; the transformation of Fe^{3+} ions into unobservable Fe^{2+} ions occurred; possibly the release of these ions from the distorted octahedral cell occurred. The signal from the defects was characterized by a g-factor of 1.9775. After roasting, the signal from the defects disappeared as expected. The structure became more balanced, and the positions of paramagnetic iron and manganese ions in the structure of silicates after roasting became equivalent.

REFERENCES

[1] H. Yang, W. Yang, Y. Hu, C. Du, A. Tang, Part. Part. Syst. Charact. **22** (2005) 207.
[2] A.I. Khatsrinov, A.V. Kornilov, T.Z. Lygina, Z.V. Mezhevich, Inorg. Mater. **55** (2019) 1138.
[3] R.E. Grim, *Applied clay mineralogy*, McGraw-Hill, New York (1962).
[4] A. Steudel, R. Kleeberg, C.B. Koch, F. Friedrich, K. Emmerich, Appl. Clay Sci. **132-133** (2016) 626.
[5] V.I. Osipov, E.M. Sergeev, Bull. Int. Assoc. Eng. Geol. **5** (1972) 9.
[6] ISO 24235, "Fine ceramics: determination of particle size distribution of ceramic powders by laser diffraction method", Int. Stand. Org. (2007)
[7] ISO 21822, "Fine ceramics: measurement of iso-electric point of ceramic powder", Int. Stand. Org. (2019).
[8] ISO 13099-2, "Colloidal systems: methods for zeta-potential determination, part 2, optical methods", Int. Stand. Org. (2012).
[9] A.G. Chetverikova, Meas. Tech. **11** (2022) 936.
[10] GOST 21216-2014, "Clay raw materials: test methods", Izd. Stand., Moscow (2015).
[11] O.N. Kanygina, V.L. Berdinskii, M.M. Filyak, A.G. Chetverikova, V.N. Makarov, M.V. Ovechkin, Tech. Phys. **65** (2020) 1261.
[12] Coll. Sci., "Determination of total calcium and magnesium ion concentration magnesium", Un. Canterbury (2017).
[13] J. Chen, F. Min, L. Liu, F. Jia, Physicochem. Probl. Miner. Process. **56** (2020) 338.
[14] O.N. Kanygina, M.M. Filyak, A.G. Chetverikova, Inorg. Mater. **54** (2018) 904.
[15] R.Z. Rakhimov, N.R. Rakhimova, A.R. Gaifullin, O.V. Stoyanov, G.I. Yakovlev, Bull. Kazan Technol. Un. **18** (2015) 67.
[16] R.Z. Rakhimov, N.R. Rakhimova, A.R. Gaifullin, Adv. Cem. Res. **29** (2017) 21.
[17] I.A. Levitskii, O.N. Horuzhik, Glass Ceram. **94** (2021) 26.
[18] V.N. Makarov, O.N. Kanygina, Nanosyst. Phys. Chem. Math. **11** (2020) 153.
[19] V.A. Kukartsev, V.V. Kukartsev, E.A. Chzhan, V.S. Tynchenko, A.A. Stupina, J. Phys. Conf. Ser. **1015** (2018) 52016.
[20] M. Baratian, M.A. Arian, A. Yazdi, GeoSaberes **11** (2020) 349.
[21] S.M. Barbosa, C.E. Carducci, M.E. Serafim, W.M. Zeviani, B. Albach, E.M. Castro, G.C. de Oliveira, Geod. Reg. **26** (2021) e00419.
[22] E. Kłosek-Wawrzyn, J. Małolepszy, P. Murzyn, Procedia Eng. **57** (2013) 572.
[23] R.T. Martin, Clays Clay Miner. **3** (1954) 117.

[24] K.M. Stack, R.E. Milliken, Icarus **250** (2015) 332.
[25] B. Tyagi, C.D. Chudasama, R.V. Jasra, Spectrochim. Acta A **64** (2006) 273.
[26] V. Ramasamy, P. Rajkumar, V. Ponnusamy, Indian J. Phys. **83** (2009) 1295.
[27] G. Jovanovski, P. Makreski, Maced. J. Chem. Chem. Eng. **35** (2016) 125.
[28] J.-U. Hahn, in "The MAK-collection part III: air monitoring methods" **13** (2012) 73.
[29] A.G. Chetverikova, O.N. Kanygina, G.Z. Alpysbaeva, A.A. Yudin, S.S. Sokabaeva, Kondens. Sredy Mezhfaznye Granitsy **21** (2019) 446.
[30] G. Jovanovski, V. Stefov, B. Šoptrajanov, B. Boev, N. Jb. Miner. Abh. **177** (2002) 241.
[31] J. Cui, Z. Zhang, F. Han, Appl. Clay Sci. **190** (2020) 105543.
[32] D. Slay, D. Cao, E.C. Ferré, M. Charilaou, J. Appl. Phys. **130** (2021) 113902.
[33] N. Worasith, B.A. Goodman, J. Neampan, N. Jeyachoke, P. Thiravetyan, Clay Miner. **46** (2011) 539.
[34] P. Hall, Clay Miner. **15** (1980) 321.
[35] J. Babińska, K. Dyrek, P. Wyszomirski, Mineral. Pol. **38** (2007) 125.
[36] G.N. Hemanthkumar, G. Parthasarathy, R.P.S. Chakradhar, I. Omkaram, R.J. Lakshmana, Y.C. Ratnakaram, Phys. Chem. Miner. **36** (2009) 447.
(Rec. 19/04/2022, Rev. 22/06/2022, Ac. 18/08/2022)